Multistage Counter-Current Crystallization for the Separation of Solid Solutions

Stephan Münzberg†, Heike Lorenz†, Andreas Seidel-Morgenstern†‡

†Max Planck Institute for Dynamics of Complex Technical Systems, Sandtorstrasse 1, 39106 Magdeburg, Sachsen Anhalt, Germany

‡Otto-von-Guericke University, Institute of Process Engineering, Chair for Chemical Process Engineering, 39106 Magdeburg, Sachsen Anhalt, Germany

While one crystallization step can be sufficient to provide pure components in case of eutectic systems, multistage operation is required to resolve solid solutions. In this work, a recently published equilibrium stage model was adopted and generalized to simplify the description of the corresponding solid-liquid equilibrium (SLE). The equilibria of the system potassium sulfate/ammonium sulfate/water were studied at 10 °C, 40 °C and 65 °C. The existence of a controversially discussed miscibility gap below 25 °C could not be confirmed. Using the equilibrium stage model and the studied specific SLE data, process variants considering different evaporation strategies were simulated.

1. Introduction

In chemical industry crystallization is not only used as a simple solid-liquid separation process, but also serves the purpose of preparing pure crystalline products. As it is generally known to be cost-effective, straightforward and broadly applicable, crystallization is of interest for a large number of industrial separation processes, devoted to provide bulk products like sugars, or highly pure active pharmaceutical ingredients [1, 2].

The class of solid solutions represents a special challenge for crystallization processes. Approximately 14 % of all known organic [3] and many more inorganic systems like alloys form solid solutions, which are characterized by inclusion of statistically distributed guest molecules in a host crystal lattice. Additionally, partial miscibility in the solid state can also occur in eutectic or intermediate compound-forming systems. However, it is difficult to spot and therefore often not recognized [4].

Solid solutions are either formed between molecules of similar size and crystal structure as a consequence of substitutionally replacement of one component by the other or by interstitially integration if one molecule is much smaller than the host molecule [5].

Special attention should be paid to the corresponding phase diagram of a solid solution forming system. In contrast to eutectic systems, tie lines in regions of miscibility do not end at pure component corners, but each solid phase composition is equilibrated with a unique liquid phase composition. Consequently, one single crystallization step is not sufficient for the generation of highly purified products, and multistage fractional crystallization processes are needed [6, 7].

These processes usually suffer from small product yields due to the separation and discard of phases that still contain product. One possible solution is to recycle usually removed phases in a counter-current manner, analogous to other purification processes like distillation, extraction or chromatography [6, 8, 9].

This process concept is already widely applied in melt crystallization, as e.g. in the Sulzer MWB process, where melts of two separation stages are mixed and circulated over a falling film crystallizer [10]. As layer thickness on the cooled surfaces increases, the liquid is pumped back into a buffer tank, followed by melting the crystallized solid and storing it in another buffer tank.

Analogously, solution crystallization can be used for substances that decompose below their melting temperature. The major difficulty for a process similar to the Sulzer MWB is the transport of crystallized material. A concept discussed recently [11, 12] takes advantage of a cascade of several interconnected batch crystallizers, in which the phases are separated by filtration. Then, solid phases are dissolved in mother liquors originating from other stages. Thus, only liquid phases are transported.

A mathematical description of the complex process of multistage counter-current crystallization as foundation of computer-based simulation of the cascade provides a valuable tool for process understanding, and the design of corresponding plants. Within this work, a previously described equilibrium model [13] was adopted and generalized in terms of applicability, transparency and simplicity. The thermodynamical description was tested and validated for the solid solution forming system of potassium sulfate and ammonium sulfate in water. The solid-liquid equilibrium (SLE) was studied at different temperatures and gave results in excellent agreement with experimental values. The existence of a previously reported miscibility gap in the system below 25 °C, which has a long history of controversially debate, was checked, but could not be confirmed. The new approach allowed rearranging the model as system of equations, allowing the characterization of independent process variables and the elucidation of their influences on all other variables. Parameter studies exploiting the equilibrium stage model were performed to analyze the impact of the evaporation profile over the cascade on the number of required separation stages. Moreover, the steady state of the multistage process was discussed using a McCabe-Thiele analogous diagram, commonly known from traditional counter-current processes.

2. Modeling

2.1. Process description and mass balancing

Multistage counter-current solution crystallization may be described as a cascade of J independently operated crystallizers working periodically [11, 12] as shown in Fig. 1. Each crystallizer j is connected to the crystallizers $j-2$ and $j+1$. After one crystallization run k the liquid phase of crystallizer $j+1$ is separated from its solid phase and used to dissolve the solid phase in crystallizer $j-1$ completely. If necessary, solid feed and solvent may be added. Subsequently, the clear solution is pumped into crystallizer j, where a new crystallization run is started. Thus, the liquid phases were transported one stage to the left, whereas solid phases were moved to the right.

(Figure 1)

In order to describe such a process to separate two components A and B with help of a solvent C, each cascade run can be divided in sub-steps, see Fig. 2 a). At the beginning of a cycle crystallizer j is filled with crystals obtained in the cascade run before ($k-1$) by crystallization in crystallizer $j-1$ (represented as s_{j-1}^{in}). In case of a feed stage solid feed is added, forming mixing point (1). Adding mother liquor gained from the crystallization in crystallizer $j+1$ in process cycle $k-1$ (represented as l_{j-1}^{in}) to (1) forms a suspension reflected by the pseudohomogenous liquid point (2). Then, this mixture is dissolved by adding pure solvent yielding solution (3). Evaporation of solvent will lead to point (4), which is supersaturated and equilibrates by crystallization along a tie line specific to (4) into a solid phase and a liquid phase (5).

(Figure 2)

The scheme in Fig. 2 b) gives an overview which masses and compositions are balanced in which sub-steps and phases. The overall partial mass balance of the counter-current stage wise operation can be expressed as

$$m_{\mathrm{l,j}}^{\mathrm{k},(5)} \cdot w_{\mathrm{n,l,j}}^{\mathrm{k},(5)} + m_{\mathrm{s,j}}^{\mathrm{k},(5)} \cdot w_{\mathrm{n,s,j}}^{\mathrm{k},(5)} = m_{\mathrm{l,j+1}}^{\mathrm{k-1},(5)} \cdot w_{\mathrm{n,l,j+1}}^{\mathrm{k-1},(5)} + m_{\mathrm{s,j-1}}^{\mathrm{k-1},(5)} \cdot w_{\mathrm{n,s,j-1}}^{\mathrm{k-1},(5)} + m_{\mathrm{s,j}}^{\mathrm{k},(1),\mathrm{Feed}} \cdot w_{\mathrm{n,s,j}}^{\mathrm{k},(1),\mathrm{Feed}} + m_{\mathrm{s,j}}^{\mathrm{k},(3),\mathrm{Solv}} \cdot w_{\mathrm{n,s,j}}^{\mathrm{k},(3),\mathrm{Solv}} - m_{\mathrm{s,j}}^{\mathrm{k},(4),\mathrm{Solv}} \cdot w_{\mathrm{n,s,j}}^{\mathrm{k},(4),\mathrm{Solv}} \quad (1)$$

with m, the mass of a phase and w, the mass fraction of a species n within the same phase. The subscript s is used for solid phases, while l stands for the liquid phase. The numbers 1 to 5 in the superscript represent the step within the crystallization cycle in which the term is used. The superscript Feed is used for externally added solid feed crystals and the term Solv in case of added solvent in the dissolution step (3) or in case of evaporated solvent in step (4).

2.2. Description of the solid-liquid equilibria

While most variables may be accessible by simple mass balances, the amount of solvent needed for complete dissolution needs further description, as well as the phase separation during the crystallization step. Based on the previous process description the crystallization step is expressed by the following mass balance

$$m_{\mathrm{l,j}}^{\mathrm{k},(4)} \cdot w_{\mathrm{n,l,j}}^{\mathrm{k},(4)} = m_{\mathrm{l,j}}^{\mathrm{k},(5)} \cdot w_{\mathrm{n,l,j}}^{\mathrm{k},(5)} + m_{\mathrm{s,j}}^{\mathrm{k},(5)} \cdot w_{\mathrm{n,s,j}}^{\mathrm{k},(5)} \quad (2)$$

or simply when using the phase ratio $\varepsilon_{\mathrm{j}}^{\mathrm{k}} = \dfrac{m_{\mathrm{l,j}}^{\mathrm{k},(5)}}{m_{\mathrm{l,j}}^{\mathrm{k},(5)} + m_{\mathrm{s,j}}^{\mathrm{k},(5)}} = \dfrac{m_{\mathrm{l,j}}^{\mathrm{k},(5)}}{m_{\mathrm{l,j}}^{\mathrm{k},(4)}}$ as

$$w_{\mathrm{n,l,j}}^{\mathrm{k},(4)} = \varepsilon_{\mathrm{j}}^{\mathrm{k}} \cdot w_{\mathrm{n,l,j}}^{\mathrm{k},(5)} + \left(1-\varepsilon_{\mathrm{j}}^{\mathrm{k}}\right) \cdot w_{\mathrm{n,s,j}}^{\mathrm{k},(5)} \quad (3)$$

The unknown compositions of liquid and the solid phases after crystallization $w_{\mathrm{n,l,j}}^{\mathrm{k},(5)}$ and $w_{\mathrm{n,s,j}}^{\mathrm{k},(5)}$, clearly depend on the specific tie line belonging to the composition after generating supersaturation $w_{\mathrm{n,l,j}}^{\mathrm{k},(4)}$.

To model the tie lines, previous works transformed the ternary phase diagram into cartesian space, where thermodynamical data, like solubility and tie lines, could be expressed as a set of two dimensional polynomials [13]. After evaluating the cartesian coordinates of resulting mother liquor and crystals, back transformation into the ternary space lead to the unknown compositions.

A more general approach uses the fact that tie lines of solid solutions do not cross each other as required by Gibbs phase rule and shown in Fig. 3. This means a liquid phase composition may be expressed as a polynomial function of its solid phase composition with degree $\mathrm{M_n}$ and coefficients $a_{\mathrm{n,m}}$ by

$$w_{\mathrm{n,l}} = f\left(w_{n,s}\right) = \sum_{m=1}^{\mathrm{M_n}} a_{\mathrm{n,m}} \cdot w_{\mathrm{n,s}}^{m} \qquad (4)$$

for the solid solution forming substances $\mathrm{n} = \mathrm{A,B}$ in solvent C, as illustrated in the quasi-binary plot in Fig. 3.

(Figure 3)

When applying the closing conditions $1 = w_{\mathrm{A,l}} + w_{\mathrm{B,l}} + w_{\mathrm{C,l}}$, $1 = w_{\mathrm{A,s}} + w_{\mathrm{B,s}} + w_{\mathrm{C,s}}$ with $w_{\mathrm{C,s}} = 0$, leads to the polynomial description of the liquid phase composition with respect to the equilibrium solid composition:

$$\begin{pmatrix} w_{\mathrm{A,l}} \\ w_{\mathrm{B,l}} \\ w_{\mathrm{C,l}} \end{pmatrix} = \begin{pmatrix} \sum_{m=1}^{\mathrm{M_A}} a_{\mathrm{A,m}} \cdot \left(1 - w_{\mathrm{B,s}}\right)^{m} \\ \sum_{m=1}^{\mathrm{M_B}} a_{\mathrm{B,m}} \cdot w_{\mathrm{B,s}}^{m} \\ 1 - w_{\mathrm{A,l}} - w_{\mathrm{B,l}} \end{pmatrix} \qquad (5)$$

Now Eq. (5) may be inserted into Eq. (3) for $\mathrm{n} = \mathrm{A,B}$ to obtain the unknown solid and the liquid phase composition after crystallization.

$$\begin{aligned} 0 &= \begin{pmatrix} \varepsilon_{\mathrm{j}}^{\mathrm{k}} \cdot w_{\mathrm{A,l,j}}^{\mathrm{k},(5)} + \left(1 - \varepsilon_{\mathrm{j}}^{\mathrm{k}}\right) \cdot w_{\mathrm{A,s,j}}^{\mathrm{k},(5)} - w_{\mathrm{A,l,j}}^{\mathrm{k},(4)} \\ \varepsilon_{\mathrm{j}}^{\mathrm{k}} \cdot w_{\mathrm{B,l,j}}^{\mathrm{k},(5)} + \left(1 - \varepsilon_{\mathrm{j}}^{\mathrm{k}}\right) \cdot w_{\mathrm{B,s,j}}^{\mathrm{k},(5)} - w_{\mathrm{B,l,j}}^{\mathrm{k},(4)} \end{pmatrix} \\ &= \begin{pmatrix} \varepsilon_{\mathrm{j}}^{\mathrm{k}} \cdot \sum_{m=1}^{\mathrm{M_A}} a_{\mathrm{A,m}} \cdot \left(1 - w_{\mathrm{B,s,j}}^{\mathrm{k},(5)}\right)^{m} + \left(1 - \varepsilon_{\mathrm{j}}^{\mathrm{k}}\right) \cdot \left(1 - w_{\mathrm{A,s,j}}^{\mathrm{k},(5)}\right) - w_{\mathrm{A,l,j}}^{\mathrm{k},(4)} \\ \varepsilon_{\mathrm{j}}^{\mathrm{k}} \cdot + \sum_{m=1}^{\mathrm{M_B}} a_{\mathrm{B,m}} \cdot \left(w_{\mathrm{B,s,j}}^{\mathrm{k},(5)}\right)^{m} + \left(1 - \varepsilon_{\mathrm{j}}^{\mathrm{k}}\right) \cdot w_{\mathrm{B,s,j}}^{\mathrm{k},(5)} - w_{\mathrm{B,l,j}}^{\mathrm{k},(4)} \end{pmatrix} \end{aligned} \qquad (6)$$

In Eq. (6), the unknown variables $\varepsilon_{\mathrm{j}}^{\mathrm{k}}$ and $w_{\mathrm{B,s,j}}^{\mathrm{k},(5)}$ are accessible directly via numerical methods. Subsequently, all other unknown variables of step (5) can be calculated.

A similar approach can be used to model the dissolution step, as illustrated in Fig. 4. When adding solvent to the pseudohomogeneus solution (2), the ratio of the mass fractions $w_{A,l}$ and $w_{B,l}$ remains constant

$$\frac{w_{B,l,j}^{k,(2)}}{w_{A,l,j}^{k,(2)}} = \frac{w_{B,l,j}^{k,(3)}}{w_{A,l,j}^{k,(3)}} \quad (7)$$

and such follows an isopleth connecting point (2) with the solvent corner of the phase diagram. Now, the composition of the dissolved solution (3) can be described by finding the tie line which intersects the isopleth and the solubility line in the same point. When inserting Eq. (5) in Eq. (7) the solid phase composition w^* of the required tie line can be received.

(Figure 4)

$$\frac{w_{B,l,j}^{k,(2)}}{w_{A,l,j}^{k,(2)}} = \frac{\sum_{m=1}^{M_B} a_{B,m} \cdot \left(w^*\right)^m}{\sum_{m=1}^{M_A} a_{A,m} \cdot \left(1-w^*\right)^m} \quad (8)$$

By introducing w^* into Eq. (5) the liquid phase composition at point (3) may be evaluated.

$$\begin{pmatrix} w_{A,l,j}^{k,(3)} \\ w_{B,l,j}^{k,(3)} \\ w_{C,l,j}^{k,(3)} \end{pmatrix} = \begin{pmatrix} \sum_{m=1}^{M_A} a_{A,m} \cdot \left(1-w^*\right)^m \\ \sum_{m=1}^{M_B} a_{B,m} \cdot \left(w^*\right)^m \\ 1 - w_{A,l,j}^{k,(3)} - w_{B,l,j}^{k,(3)} \end{pmatrix} \quad (9)$$

This generalized approach describing the process' thermodynamics was found to be more stable when formulating the process as a system of equations than the previously reported method of transformation into the cartesian space. The practicability of the approach was evaluated for the SLE of potassium sulfate/ammonium sulfate in water described below.

3. Experimental

3.1. Materials

Potassium sulfate (K_2SO_4) was purchased from Carl Roth GmbH & Co (Germany, purity 99 %+), while ammonium sulfate ($(NH_4)_2SO_4$) was obtained from Sigma-Aldrich (Germany, purity 99 %+). Both were used as received. Water, which was purified by a Milli-Q gradient system from Millipore Corporation (France), was used as solvent. Ethanol (99 %+), purchased from VWR International, was used to wash obtained crystals. Methanolsulfonic acid, purchased from Sigma-Aldrich, sodium carbonate and sodium bicarbonate received from Merck (Germany) were used for ion chromatography analysis.

3.2. Solid-liquid equilibria studies of potassium sulfate and ammonium sulfate in water

The system $K_2SO_4/(NH_4)_2SO_4/H_2O$ was characterized previously and SLE data can be found in literature [12, 14-18]. Most data reported suggest the system to form solid solutions over the whole range of compositions [12, 14, 16]. Nevertheless, few publications indicate for the system a narrow miscibility gap [15, 17, 18].

To check the existence of this miscibility gap and to verify literature data, solubility measurements were performed isothermally at 10 °C, 40 °C and 65 °C. Precalculated amounts of K_2SO_4 and $(NH_4)_2SO_4$ were weighed into vials containing a magnetic stirrer. 15 ml of water were added to the samples and the vials were sealed. The sealed vials were thermostated in a water filled double jacketed beaker connected to a Lauda E100 thermostat and stirred electromagnetically at 700 rpm. Samples were first dissolved at 65 °C for the 10 °C and 40 °C experiment and at 80 °C in case of the 65 °C experiment. After clear solution was reached, the vials were cooled down to the desired final temperature and equilibrated for at least 72 hours. The equilibrated liquid phase was sampled by a heated syringe and filter to avoid nucleation. Then, the solid phase was filtrated using underpressure and washed with ethanol.

Both, solid and liquid phase composition, were analyzed via ion chromatography. To verify the formation of mixed crystals, the solid phase was studied by X-Ray powder diffraction.

3.3. Analytical methods

Compositions were analyzed using an ion chromatography (IC) system DIONEX ICS-1100 equipped with IonPac CS (3x250 mm) column and IonPac ASS22 (4x250 mm) columns for cation and anion analyses, respectively. Solid and liquid samples were diluted with MilliQ-water. The measurement conditions were as follows.

Cations: eluent = 30 mM methanesulfonic acid at 0.40 ml/min. Anions: 3.3 µM Na_2CO_3/0.3 µM $NaHCO_3$ at 1.20 ml/min. Temperature was set to 25 °C. Injected volume was 50 µl.

X-Ray powder diffraction analyses (XRPD) were performed using a PANalytical X'PERT PRO diffractometer (Netherlands), applying $Cu_{K\alpha}$ radiation and an X'Celerator detector. Data were collected in 2θ range of 15° to 40° using a step size of 0.008 °/step and a collection time of 60 s/step.

4. Results and discussion

4.1. SLE of potassium sulfate and ammonium sulfate in water

SLE data were measured at 10 °C, 40 °C and 65 °C. The measured solubilities in the potassium sulfate/ammonium sulfate/water system at the studied temperatures are shown in Fig. 5. Solubility isotherms at all observed temperatures show a similar trend of steadily increasing solubilites from the lower soluble potassium sulfate towards ammonium sulfate. This behavior is in good agreement with reported literature data, e.g. [12, 14-18].

(Figure 5)

While Fig. 6 a) illustrates the measured SLE data at 10 °C in a ternary representation, Fig. 6 b) shows the translation of the SLE data into its quasi-binary representation. When plotted over the solid phase composition, both, the potassium sulfate and the ammonium sulfate mass fractions in the liquid phase may be described with a high degree of accuracy by third order polynomials. Corresponding parameters are given for all temperatures in Tab. 1.

(Figure 6)

(Table 1)

With an increasing amount of ammonium sulfate in the solid phase, the liquid phase enriches in ammonium sulfate as well. On the contrary, the mass fraction of potassium sulfate in the liquid phase is decreasing. The solubility, represented by the calculated mass fraction of water in the liquid phase, is decreasing strongly for solid phases poor in ammonium sulfate (<50 wt%). A similar trend is found for solid phases rich in ammonium sulfate (>85 wt%). Additionally, an intermediate region between 50 wt% ammonium sulfate and 85 wt% percent in the solid state could be detected in which solubility seems to be constant.

In the ternary phase diagram shown in Fig. 6 a), this region is represented by a number of tie lines, starting from different compositions in the solid phase and approaching a specific point on the solubility line.

Additionally, the SLE may be expressed as a distribution diagram, analogously to other purification techniques, as distillation or extraction. Therefor a distribution coefficient

$$k = \frac{w_{\mathrm{B,l}}}{w_{\mathrm{A,l}} + w_{\mathrm{B,l}}} \qquad (10)$$

with the mass fractions of A and B in the liquid phase can be defined. When plotted against the mass fraction of B in the solid phase, k is a measure of the slope of the tie lines. Therefore, the efficiency of a single crystallization step may be estimated by the deviation of the distribution curve from the 45° line.

The distribution plot of the observed potassium sulfate/ammonium sulfate/water system is shown in Fig. 7 including the data at all three studied temperatures 10 °C, 40 °C and 65 °C. As can be seen, all distributions lie continously above the 45° line. Thus, over the entire composition region ammonium sulfate enriches in the liquid phase, while potassium sulfate in the solid phase.

(Figure 7)

The temperature was found to significantly influence the distribution coefficient. Higher temperatures compressed the curve towards the 45° line, making a separation process more demanding, due to a less efficient tie line slope.

As emphasized before, in literature the existence of a peritonic miscibility gap is still discussed. In case of such a miscibility gap, a certain liquid phase composition is in equilibrium with a range of solid phase compositions [17, 18]. Even if the ternary phase

diagram in Fig. 6 indicates the existence of a miscibility gap (magnified area), its presence is not clearly visible due to the triangular shape of the phase diagram. The distribution coefficient plot can be used to check the existence more precisely. There, the described miscibility gap would occur as section with constant k.

In order to clarify the existence, we checked the SLE at 10 °C in more detail. Based on previous experiments, we expected the miscibility gap, if present, to occur in the region of 69.5 wt% to 72.5 wt% ammonium sulfate. This region is plotted in the distribution plot in Fig. 7 as magnified area, where it becomes clear the distribution coefficient is monotonical increasing. Also no indications of the occurrence of a miscibility gap was found in XRPD patterns of the corresponding solid phases. Therefore we cannot confirm the existence of this miscibility gap.

4.2. Process simulation study

Lin et al. [19] already investigated some idealized operating modes for counter-current crystallization cascades. It was suggested that steady state operation can be described analogously to the McCabe-Thiele theory, but requires the solvent content in the liquid phase to be constant over the cascade. If, as in our case, addition of solvent in each stage is needed to dissolve the solid phase fully, the generation of supersaturation by evaporation is a promising approach for selecting tie lines to be used and therefore controlling the equilibria in all stages in the cascade. In contrast to the approach given in [19], operating lines are in this case not necessarily straight. Hence, simple graphical solutions are not accessible.

For improved understanding of the whole dynamics of the process sequence simulations were performed in particular regarding the influence of the required evaporation factor δ, which can alter the specific tie line.

$$\delta_{\mathrm{j}} = \frac{m_{\mathrm{l,j}}^{\mathrm{k},(4),\mathrm{Solv}}}{m_{\mathrm{l,j}}^{\mathrm{k},(3)} \cdot w_{\mathrm{C,l,j}}^{\mathrm{k},(3)}} \qquad (11)$$

In Eq. (11) $m_{\mathrm{s,j}}^{\mathrm{k},(4),\mathrm{Solv}}$ is the evaporated solvent mass in crystallizer j and $\mathrm{m}_{\mathrm{l,j}}^{\mathrm{k},(3)} \cdot w_{\mathrm{C,l,j}}^{\mathrm{k},(3)}$ corresponds to the total solvent mass after dissolution.

As model system evaporation crystallization of the previously described anorganic potassium sulfate/ammonium sulfate/water at 65 °C with a solid feed composition of 50 %/50 % was chosen. The objective function was defined as $\mathrm{Pu}_{\mathrm{A,s,J}} \geq 0.98 \cap \mathrm{Y}_{\mathrm{A,s,J}} \geq 0.8$ with the purity of A in the crystallized solid phase in crystallizer J

$$\mathrm{Pu}_{\mathrm{A,s,J}} = \frac{w_{\mathrm{A,s,J}}^{\mathrm{k}\to\infty,(5)}}{w_{\mathrm{A,s,J}}^{\mathrm{k}\to\infty,(5)} + w_{\mathrm{B,s,J}}^{\mathrm{k}\to\infty,(5)}} \qquad (12)$$

and the current yield of A

$$\mathrm{Y}_{\mathrm{A,s,J}} = \frac{m_{\mathrm{s,J}}^{\mathrm{k}\to\infty,(5)} \cdot w_{\mathrm{A,s,J}}^{\mathrm{k}\to\infty,(5)}}{\sum_{\mathrm{j=1}}^{\mathrm{J}} m_{\mathrm{s,j}}^{\mathrm{k}\to\infty,(1),\mathrm{Feed}} \cdot w_{\mathrm{A,s,j}}^{\mathrm{k}\to\infty,(1),\mathrm{Feed}}} \qquad (13)$$

in steady state ($k \to \infty$). In this parametric simulation study the addition of feed was controlled such that the feed crystallizer always contained a total mass of 1 kg after dissolution (point 3 in Fig.2 a)).
Due to the repeated dissolution and evaporation procedure, minimization of separation stages will not only decrease plant complexity, but also optimize the evaporation effort, defined as

$$E = \frac{\sum_{j=1}^{J} m_{l,j}^{k\to\infty,(3),Solv}}{\sum_{j=1}^{J} m_{s,j}^{k\to\infty,(1),Feed} \cdot w_{A,s,j}^{k\to\infty,(1),Feed}} \qquad (14)$$

mass of evaporated solvent over the cascade, divided by added feed.
To identify an optimal process configuration a systematic parameter variation was used. Given a number of crystallizers J, all possible feed positions were tested. In case the objective function was fulfilled by one or more setups, the optimal configuration was chosen as the one with the lowest evaporation effort. If none of the configurations met the objective function, the number of crystallizers J was increased by one and the test was repeated. Results of the simulations are given in Tab. 2.

(Table 2)
In cases A, B and C, the profiles were set to a constant value over the whole cascade as seen before [12]. Fig. 8 a) shows exemplarily the steady state equilibrium for case A, using a cascade configuration with seven crystallizers, in which the feed is added in stage 6 and $\delta_j = 0.5$. Obviously, this evaporation profile tends to have barely effective separation stages (stage 3 to 6), where tie lines in neighbored crystallizers lie close to each other. The upper plot in Fig. 9 a) shows a McCabe-Thiele type diagram of case A based on the distribution plot described above. Similar to distillation or extraction processes, the stage efficiency of the purification can be illustrated by the length of vertical and horizontal steps. While stages 1, 2 and 7 are characterized by wide or at least moderate steps, stages 3 to 6 are shorter.
(Figure 8)
(Figure 9)
In case B evaporation factor δ_j was increased to 0.6 over the whole cascade. The optimal process configuration was found for a cascade with 5 crystallizers in which feed was added in crystallizer 3. Steady state equilibrium showed a significant improvement of stage efficiency, resulting in a lower number of separation stages.
Case C used an evaporation factor of 0.7. The cascade's equilibrium was pushed in this case towards highly pure mother liquor containing ammonium sulfate and could not manage to provide the necessary purity of potassium sulfate in the solid phase for a reasonable number of separation stages.
Further optimization potential of the cascade can be achieved when the evaporation is set independently for each stage such that step sizes in the McCabe-Thiele analogous diagram increase. Case D shows a flexible evaporation profile in which δ_j is varied such, that crystallization in the separation stages is in accordance with a set of arbitrarily predefined, well distributed, tie lines. Compared to the distribution of A

shown in Fig. 9 a), the steps in case D are distributed more equal and distant to each other than in case A. Due to the exact definition of tie lines, four separation stages are sufficient for the concrete separation process considered. Therefore the evaporation effort decreases by almost 50 % compared to case A and 37 % to case B, as visible in Tab. 2.

The development of specifically optimized δ_j values over the process cycles k is shown in Fig. 9 b). With these values the process reaches the steady state within less than 18 cycles. The profile in the crystallizers at the cascade ends ($j=1$ and $j=4$) was found to be constant after their first adjustment. This was to be expected, as both crystallizers were fed with just one phase, either liquid or solid, with a fixed composition from their neighboring crystallizers. Hence, the other crystallizers have to balance changing input masses. This fact leads initially to an overshoot of δ_j values in crystallizers $j=2$ and $j=3$ compared to their steady state value as shown in Figure 9 b), which disappears within a few cycles. In summary, the evaporation strategy was found to be a crucial, but valuable tuning parameter for process improvement, for which deeper analysis is underway.

5. Conclusion

This work provided an improved theoretical description of a counter-current crystallization process capable to resolve solid solutions. A specific separation problem was studied partly experimentally with respect to the key information needed for process design, namely the solid-liquid equilibria. As a model system the solid solution forming mixture of potassium sulfate and ammonium sulfate dissolved in water was chosen. Full miscibility in the solid state was verified. Based on the measured equilibrium data, the influence of supersaturation on the stage numbers required was analyzed theoretically. For this, stage specific evaporation factors were evaluated. Both, high and low but constant evaporation factors were found to be not attractive. A strategy to identify for each stage adjusted evaporation factors was developed and found to be very promising.

Symbols used

Symbols

a		Polynomial coefficients for SLE description
E	$\left[\mathrm{kg_{Solv}\ kg_{Feed}^{-1}}\right]$	Evaporation effort
m	$\left[\mathrm{kg}\right]$	Mass
Pu	$\left[\mathrm{kg_{pure\ Prod}\ kg_{total\ Prod}^{-1}}\right]$	Purity
T	$\left[\mathrm{°C}\right]$	Temperature
w	$\left[\mathrm{wt\%}\right]$	Mass fraction
Y	$\left[\mathrm{kg_{Prod\ collected}\ kg_{Feed\ added}^{-1}}\right]$	Yield

Greek symbols

δ	$\left[\mathrm{kg}_{\text{evap. Solv}}\ \mathrm{kg}^{-1}_{\text{total Solv}}\right]$	Evaporation factor
ε	$\left[\mathrm{kg}_{\text{Liq}}\ \mathrm{kg}^{-1}_{\text{total}}\right]$	Phase ratio

Sub- and Superscripts

Feed	Added Feed
j	Index of cascade stage 1 … J
k	Process cycle
l	Liquid phase
m	Degree of polynomial term
n	Components A, B, C
s	Solid phase
Solv	Added or evaporated Solvent

References

[1] W. Beckmann, *Crystallization: Basic concepts and industrial applications*. Wiley-VCH, Weinheim, **2013**.

[2] H. Lorenz, A. Seidel-Morgenstern, *Angew. Chem. Int. Ed.* **2014,** *53 (5)*, 1218–1250. DOI: 10.1002/anie.201302823.

[3] M. Matsuoka, in *Advances in industrial crystallization*, Eds: J. Garside, R. Davey, A. G. Jones, J. W. Mullin), Butterworth Heinemann, Oxford, Boston **1991**, 229–244.

[4] H. Lorenz, in *Crystallization*, (Ed: W. Beckmann), Wiley-VCH, Weinheim **2013**, 35–74.

[5] A. I. Kitaigorodsky, *Mixed Crystals*. Springer Series in Solid-State Sciences, 0171-1873, Vol. 33, Springer Berlin Heidelberg, Berlin, Heidelberg, **1984**.

[6] G. Matz, *Chem. Ing. Tech.* **1980,** *52 (7)*, 562–570. DOI: 10.1002/cite.330520704.

[7] J. W. Mullin, *Crystallization*. 4th ed., Butterworth-Heinemann, Oxford, Boston, **2001**.

[8] P. C. Wankat, *Equilibrium staged separations: Separations in chemical engineering*. Elsevier, New York, **1988**.

[9] J. Nowak, D. Antos, A. Seidel-Morgenstern, *J. Chrom. A* **2012,** *1253*, 58–70. DOI: 10.1016/j.chroma.2012.06.096.

[10] J. Ulrich, in *Crystallization*, (Ed: W. Beckmann), Wiley-VCH, Weinheim **2013**, 325–335.

[11] D. Grawe, R. Eilers, S. Gliesing (Hapila GmbH), *DE102008023833 B4*, **2013**.

[12] E. Temmel, S. Wloch, U. Müller, D. Grawe, R. Eilers, H. Lorenz, A. Seidel-Morgenstern, *Chem. Eng. Sci.* **2013,** *114*, 662–673. DOI: 10.1016/j.ces.2013.09.054.

[13] E. Temmel, U. Müller, D. Grawe, R. Eilers, H. Lorenz, A. Seidel-Morgenstern, *Chem. Eng. Technol.* **2012,** *35 (6)*, 980–985. DOI: 10.1002/ceat.201200002.

[14] C. Calvo, E. L. Simons, *J. Am. Chem. Soc.* **1952,** *74 (5)*, 1202–1203. DOI: 10.1021/ja01125a019.

[15] N. I. Nikurashina, K. K. Il'in, *Russ. J. Inorg. Chem.* **1970,** *15 (7)*, 994–996.

[16] V. G. Shevchuk, V. N. Pilipchenko, *Russ. J. Inorg. Chem.* **1970,** *15 (1)*, 109–111.

[17] B. Dejewska, *Cryst Res Technol* **1990,** *25 (12)*, 1485–1495. DOI: 10.1002/crat.2170251221.

[18] A. Chmarzyński, *J. Mol. Liq.* **2002,** *95 (3)*, 329–338. DOI: 10.1016/s0167-7322(01)00298-7.
[19] S. W. Lin, K. M. Ng, C. Wibowo, *Comput. Chem. Eng.* **2008,** *32 (4-5)*, 956–970. DOI: 10.1016/j.compchemeng.2007.04.005.

Tables

Table 1: Parameters used to describe the measured SLE data according to Eq. (5).

	K_2SO_4			$(NH_4)_2SO_2$		
T in °C	10	40	65	10	40	65
$a_{n,1}$	0.126	0.179	0.195	1.697	1.612	1.636
$a_{n,2}$	-0.185	-0.299	-0.291	-2.629	-2.373	-2.326
$a_{n,3}$	0.139	0.246	0.247	1.363	1.218	1.174
R^2	0.996	0.999	0.989	0.992	0.997	0.997

Table 2: Steady state results of the dynamic process simulation for 4 different evaporation profiles.

Case	δ_j (–)	J / J_{Feed}	$Pu_{A,s,J}$ (–)	$Y_{A,s,J}$ (–)	E (–)
A	0.5	7/6	0.99	0.82	18.54
B	0.6	5/3	0.99	0.85	15.26
C	0.7		No solution found for $J \leq 20$		
D	See Fig. 9	4/3	0.98	0.80	9.38

1 **Figures**

2

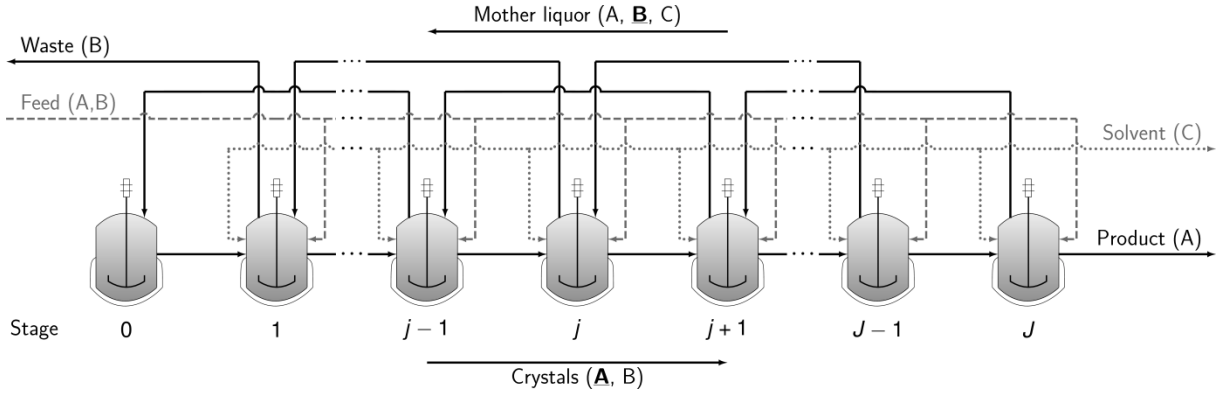

Figure 1: Scheme of a batch crystallizer cascade with *J* crystallizers for multistage solution crystallization for the separation of impure feed containing components A and B, in which mother liquor and crystals flow in a counter-current regime.

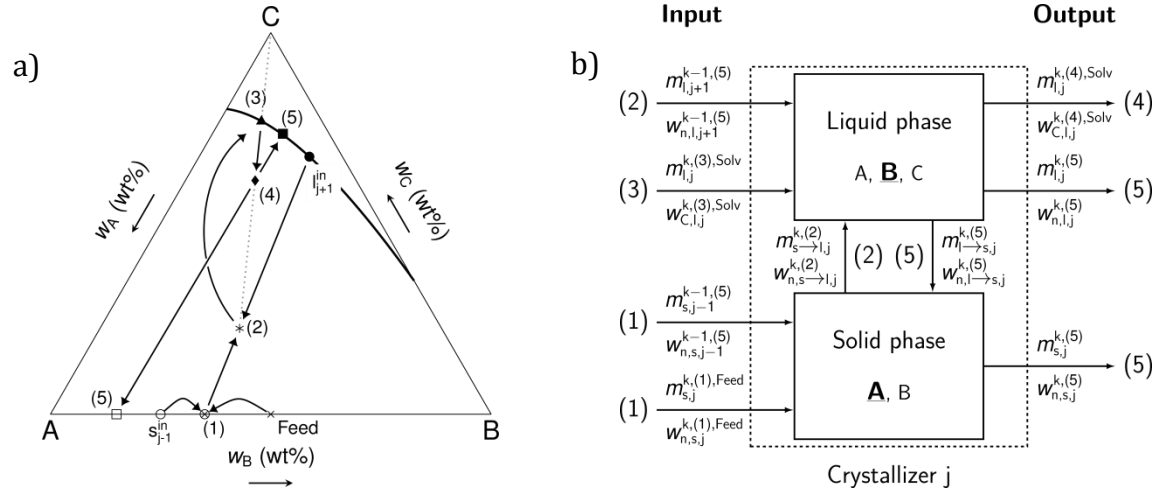

Figure 2: a) Process trajectory of one single crystallization run with solid and liquid input within the ternary phase diagram. b) Incoming and outgoing masses around crystallizer unit j, as well as phase changes between solid and liquid phases in respect to the 5 steps per crystallization run.

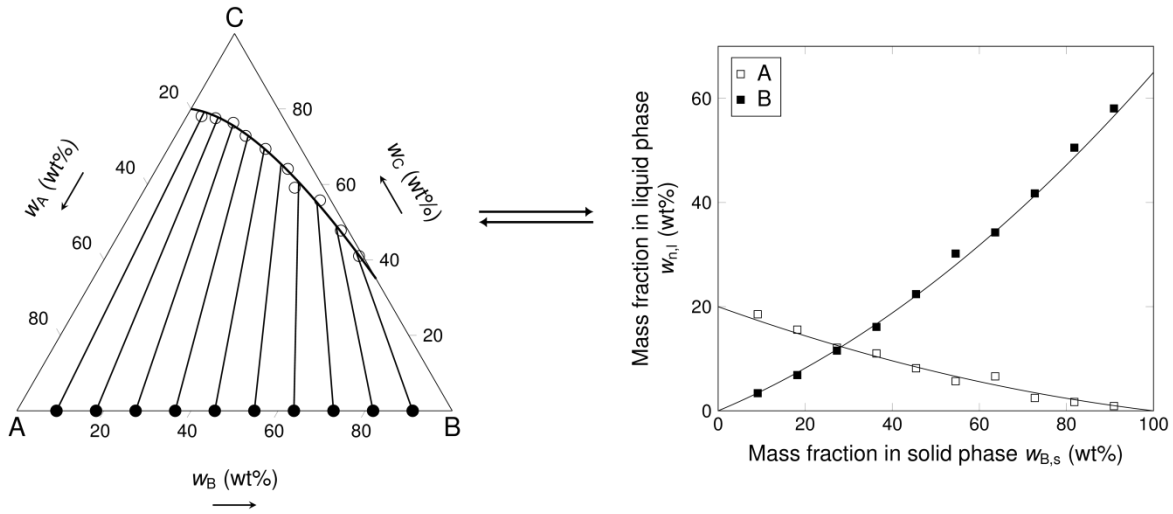

Figure 3: Ternary SLE in case of a generic phase diagram (○ Pseudo experimental liquid phase composition. ● Pseudo experimental solid phase composition) and its quasi-binary representation, based on the mass fraction of A and B in the liquid phase versus the solid phase content of B.

1

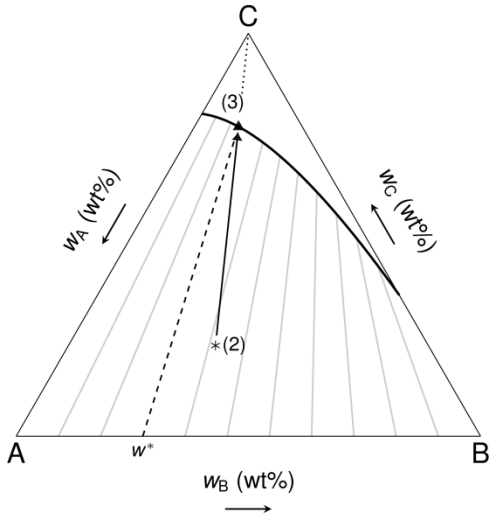

Figure 4: Relationship between the dissolution of a supersaturated mixture by addition of solvent and tie lines.

2

3

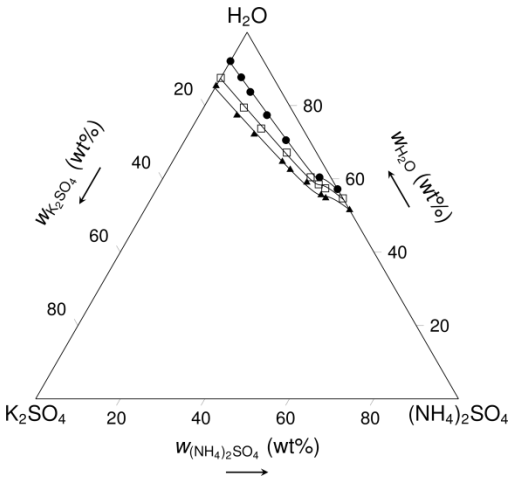

Figure 5: Solubility of the solid solutions forming system potassium sulfate/ammonium sulfate/water at 10 °C (●), 40 °C (□) and 65 °C (▲) in the ternary phase diagram.

1

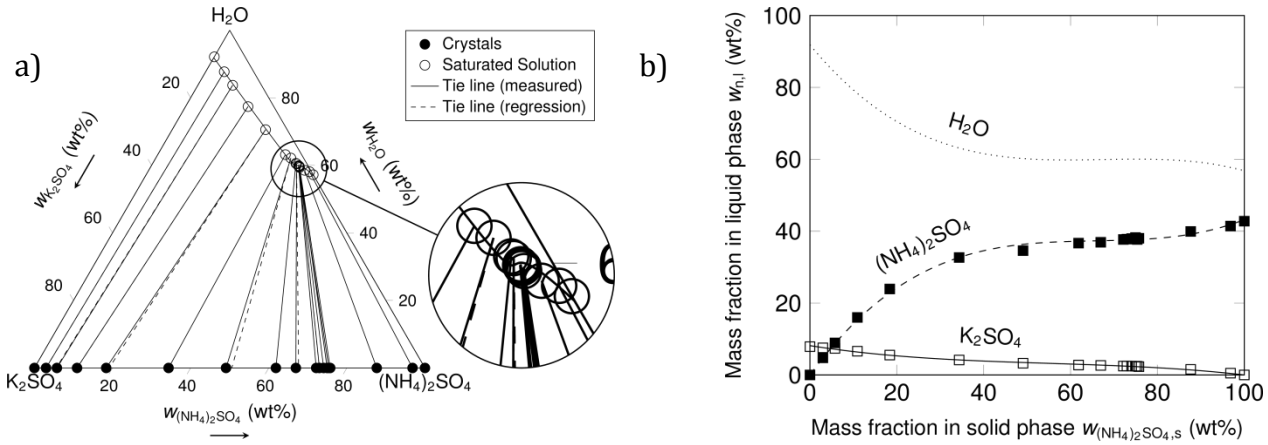

Figure 6: a) Ternary phase diagram of potassium sulfate/ammonium sulfate/water at 10 °C. Magnified area corresponds to the region of the hypothesized miscibility gap. b) Quasi-binary representation of the SLE data. Solid and dashed lines refer to the polynomial regression given in Eq. (5).

2

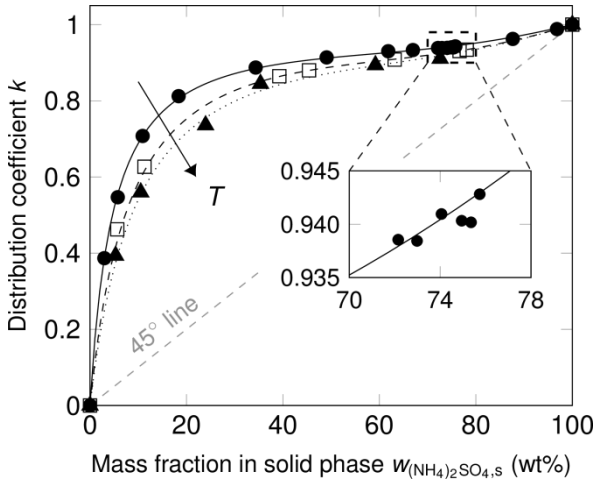

Figure 7: Distribution plot for the SLE data. Magnification shows the analysis of the proposed miscibility gap. –●– 10 °C -□- 20 °C ···▲··· 30 °C

1

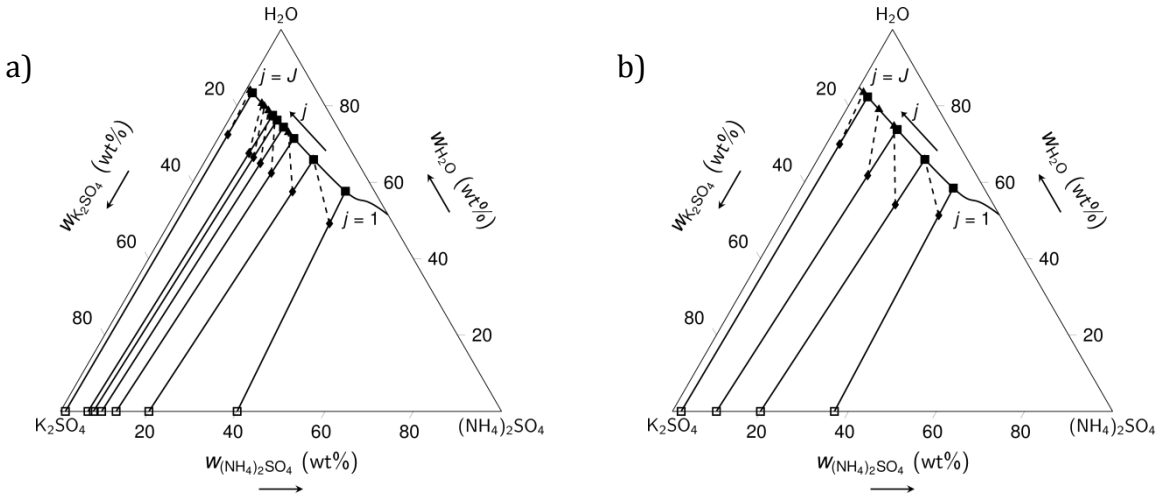

Figure 8: Results of the simulation in steady state using evaporation rates of a) $\delta_j = 0.5$ of case A and b) the complex profile of case D, in which evaporation was controlled to meet predefined tie lines. ▲ Composition after dissolution, ◆ after evaporation, ■ liquid after crystallization and □ solid. Dashed line: Isopleth for evaporation. Solid line: Tie line used for crystallization.

2

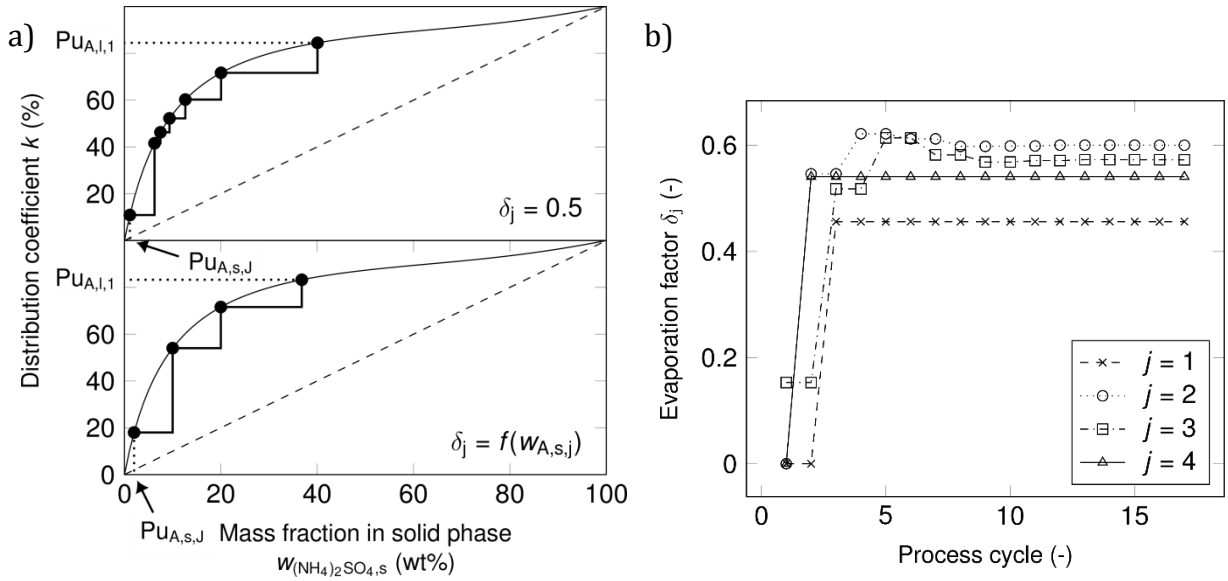

Figure 9: a) Steady state equilibrium of case A (above) and D (below) in a McCabe-Thiele analogous distribution plot. Separation stages are counted from the right to the left. b) Evolution of the evaporation profile in case D until steady state is reached in cycle 18.